Jay Ryan U. Roldan
Department of Computer Engineering,
University of California Santa Cruz,
Santa Cruz, CA 95064
e-mail: juroldan@soe.ucsc.edu

Dejan Milutinović
Department of Computer Engineering,
University of California Santa Cruz,
Santa Cruz, CA 95064
e-mail: dejan@soe.ucsc.edu

Zhi Li
Department of Electrical and
Computer Engineering,
Duke University,
Durham, NC 27708
e-mail: zhi.li2@duke.edu

Jacob Rosen
Department of Mechanical Engineering,
University of California Los Angeles,
Los Angeles, CA 90095
e-mail: jacobrosen@ucla.edu

A Low-Dimensional Dissimilarity Analysis of Unilateral and Bilateral Stroke-Impacted Hand Trajectories

In this paper, we propose a quantitative approach based on identifying hand trajectory dissimilarities through the use of a multidimensional scaling (MDS) analysis. A high-rate motion capture system is used to gather three-dimensional (3D) trajectory data of healthy and stroke-impacted hemiparetic subjects. The mutual dissimilarity between any two trajectories is measured by the area between them. This area is used as a dissimilarity variable to create an MDS map. The map reveals a structure for measuring the difference and variability of individual trajectories and their groups. The results suggest that the recovery of hemiparetic subjects can be quantified by comparing the difference and variability of their individual MDS map points to the points from the cluster of healthy subject trajectories. Within the MDS map, we can identify fully recovered patients, those who are only functionally recovered, and those who are either in an early phase of, or are nonresponsive to the therapy. [DOI: 10.1115/1.4033836]

1 Introduction

Stroke is the number one cause of long-term disability in the U.S. [1]. While it is known that the functionality of the impaired limb can be recovered through rehabilitation therapies, they come with a high price; it is an annual cost of $34 billion each year [1]. Improving rehabilitation and streamlining it toward patient-specific needs are important to expedite the recovery progress and improve its outcome.

The difficulty of recovery progress tracking during rehabilitation therapies is a major roadblock in establishing proper therapeutic plans [2]. Over the years, a wide spectrum of clinical assessment tests and tools were developed to evaluate the current state of a patient's sensory and motor performance as well the outcome of a rehabilitation treatment. Among the methods are action research arm test [3,4], arm mobility arm test [5], ashworth scale [6], assistive technology device predisposition assessment [7], box and block test [4], Canadian Occupational Performance Measure (COPM) [8], Fugl Meyer (FMA) [4,9], motor activity log [10], motor assessment scale [11], nine-hole peg test [12], and wolf motor function test (WMFT) [13]. These assessments are primarily subjective assents [14–16] that may or may not require prior training. In particular, the FMA assessment tool ranks the performance of a patient during a series of tasks on a discrete scale of 0,1,2. The patient needs to improve by 33% in order to be ranked higher on the scale. As such, this scale is not sensitive enough to changes that may result from a rehabilitation treatment.

In tracking the changes, the sensitivity is not the only factor. A method of tracking should be able to distinguish the progress in the direction of recovery toward healthy motions [17,18] from the direction in which subjects use compensatory strategies to achieve motion goals. The latter is not the goal of successful recovery plans, since though the subjects may be able to perform some daily activities, their motions would be different from those of healthy subjects.

In this paper, we present a quantitative approach to aid the tracking of recovery during a rehabilitation process using high-rate motion capture system data. The approach is focused on the quality of movements and task performance of the end effector [18]. In the process of developing the approach, we analyzed reaching trajectories of healthy and stroke-impacted hemiparetic subjects. The analysis relies on reaching trajectories, therefore, all the subjects in our study were screened for their capability of performing such tasks. We first focused on trajectory characteristics in the vertical direction and used only the z-axis component of the data. This provided information about the complexity of trajectories and showed that for a better insight into the data, a more complete analysis of trajectories is required.

The method of analysis of the trajectories proposed in this paper is MDS [19,20]. The MDS method has been used in various studies as a tool for clustering and characterizing the evolution of certain parameters [21–23]. It proved to be particularly useful for the analysis of lab assays producing data on a real-valued approximate dissimilarity measure, which is of a type that is generally considered unsuitable for quantitative analyses [24].

In this paper, the area between hand trajectories is introduced as an approximate measure of trajectory dissimilarities. Based on the measure, the MDS produces a map in which each trajectory is represented by a point. The distance between any two points of the MDS map reflects the dissimilarity of the corresponding two trajectories; therefore, the map reveals the structure of dissimilarities among trajectories. In every MDS map depicting dissimilarities among trajectories for reaching a specific target we are able to identify a dense cluster of points corresponding to healthy trajectories. Trajectories of hemiparetic subjects are usually spread over the map and we can quantify their difference and variability with respect to the cluster of healthy trajectories. In this way, the difference and variability of trajectories are quantified and can be followed on scales that are fully compatible with the observed data. Our analysis includes trajectories from healthy and hemiparetic subject groups, and the results are compared to trajectories of a single subject from the hemiparetic subject group.

The paper is organized as follows: The data collection and experiment protocol are explained in Sec. 2. Section 3 describes the methods and results of the vertical component analysis. The

Contributed by the Dynamic Systems Division of ASME for publication in the Journal of Dynamic Systems, Measurement, and Control. Manuscript received December 6, 2015; final manuscript received May 3, 2016; published online July 13, 2016. Assoc. Editor: Xiaopeng Zhao.

methods and results of the MDS analysis are detailed in Sec. 4. Section 5 provides a discussion of our results and their interpretation. Section 6 concludes the paper.

2 Data Collection and Protocol

The data were captured using a Vicon motion capture [25] system with ten cameras. Nine infrared reflective markers were attached to the left and right arm of the subjects, see Fig. 1. Since some stroke-impacted hands are characterized by flexed wrist and clenched fist, the subjects held a T-shaped pointer with a marker attached at the tip (Fig. 1(*b*)). Additional four markers were attached to the subjects' torsos and backs for a total of 24 markers. The Vicon's BODYBUILDER [26] software was used to create a biomechanical model of the arms and torsos. The motion capture system captured data at a sampling rate of 100 Hz with submillimeter accuracy. The subjects were seated, and cameras were positioned at the ceiling pointing directly toward the subjects. The experiment protocol is approved by the University of California, Santa Cruz Institutional Review (DHHS IRB Registration No. IRB00000266, #HS 1821).

Ten subjects composed the control group, and nine unhealthy, hemiparetic subjects participated in the experiments. Both subject groups underwent a screening process prior to participating in the study. For the control group, both arms had to be injury free and without any pain or discomfort. The hemiparetic group was composed of stroke survivors in their chronic phase with a disability lasting more than 2 months since they had stroke. They were able to perform reaching movements with observable impairment. Specifically, with their impaired arm, the subjects were capable of: (1) bending the elbow at 90 deg without support and keeping it there; (2) reaching up and touching their ears; (3) moving the wrist up and down; (4) grasping objects; and (5) raising the arm in front at 90 deg with the thumb pointing up.

Out of the nine subjects, only eight were included in the analysis. One of the subjects had difficulty of reaching the targets that are above the shoulder (R3 and L3, see Fig. 2). Both subject groups performed reaching tasks to targets in a 3D workspace. The workspace and targets are shown in Fig. 2. During the experiment, each subject sat on a chair with their torso straight and both hands resting on the chair handles (Fig. 1(*a*)). The chair was positioned so that the subjects could comfortably reach all the ipsilateral targets. According to the experimental protocol, the subjects were instructed to start each arm movement from a position where their hands were rested on the handles of the chair (Fig. 1(*a*)), whereas the wrist positions of the hands were aligned with the end of the chair handles. Two modes of reaching tasks were performed: unilateral and bilateral. For the unilateral mode, the subjects were asked to reach targets R1–R5 using their right hand, and then L1–L5 using their left hand. For the bilateral reaching mode, the subjects were instructed to reach simultaneously symmetric targets in the workspace. There were five repetitions for each target in both modes for a total of 25 trajectories. This resulted in 50 trajectories per subject for the right and left arms of the control group, 50 trajectories per subject for the impaired and healthy arms of the unhealthy, hemiparetic group, and 50 trajectories per subject for the bilateral reaching mode. In both unilateral and bilateral modes, the subjects were instructed to perform the reaching motion after a sound signal. Reaching motions were performed at speed comfortable to the subjects. To avoid fatigue, the subject were given time to rest between the reaching motions.

Our trajectory data are sequences of all the trajectory point coordinates from the initial hand position to the time point at which the subject touched the target with the tip of the pointer.

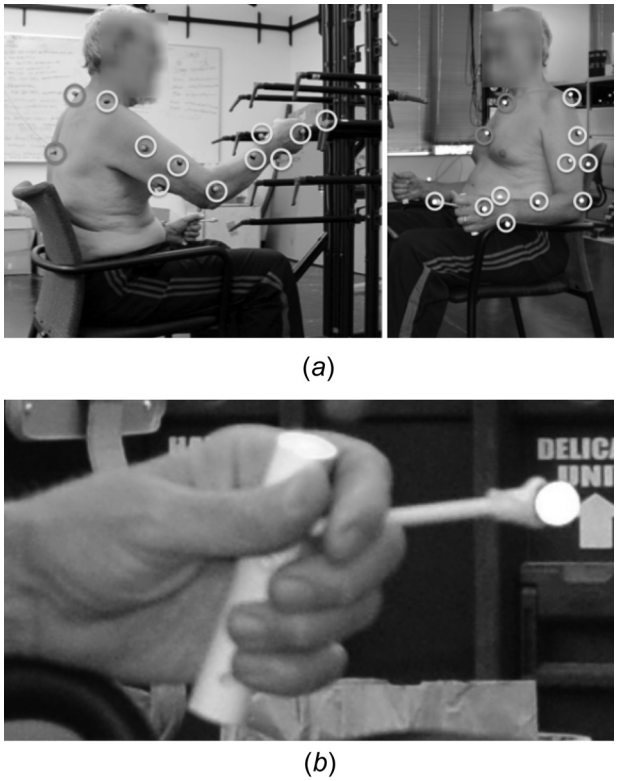

(*a*)

(*b*)

Fig. 1 Marker placement: (*a*) nine reflective markers are attached to each of the left and right arms (light gray circles). Four markers are attached to the torso (dark gray circles). (*b*) Subject holds a T-shaped pointer with a marker attached at the tip.

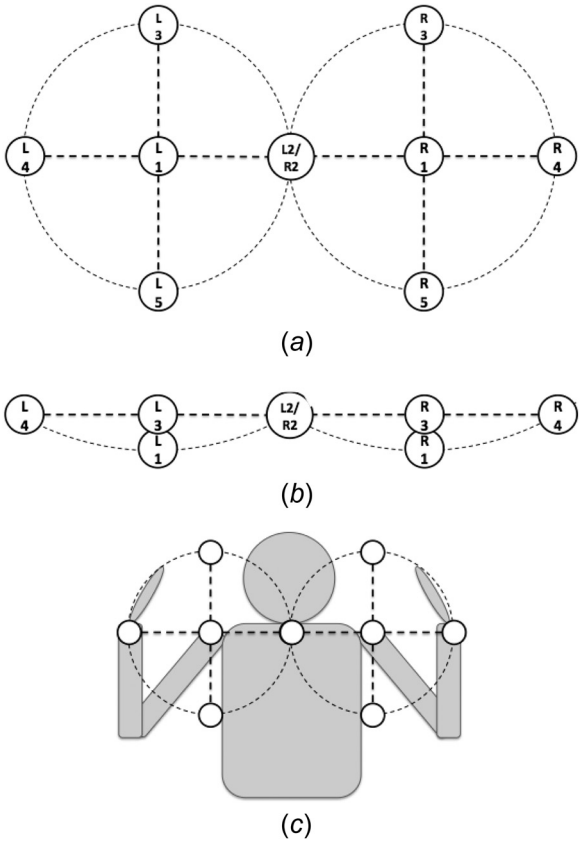

Fig. 2 Target workspace setup: (*a*) front and (*b*) top view of the target workspace. The left workspace is composed of targets L1–L5, and the right one is composed of targets R1–R5. (*c*) The subject's shoulders are aligned with the center of the left and right workspaces.

The subjects were oriented to face the positive y-axis with their right side toward the positive x-axis direction of the reference coordinate frame. Examples of the collected trajectory data are shown in Fig. 3.

3 Analysis of the Vertical (z-Axis) Component of Human Hand Trajectories

Unconstrained human reaching trajectories to a target are not straight lines. From the collected data, one of the observed characteristics is that some subjects put more emphasis on upward motion at the beginning of their trajectories and then move their hands toward the target. Because of that, we first analyzed the z-axis profile of hand trajectories using two methods. The first is the *area ratio* method, which is based on the ratio of the areas above and below the trajectory (see Fig 4). The second is the *polynomial fit* method, which is based on a polynomial model of the hand trajectory.

For the *area ratio* data analysis, the data are first normalized based on the task completion measured by the travel distance to reach the target. The areas a_a above and a_b below the trajectory are calculated as a sum of products of the increments ΔS_k of the traveled distance S in the xy-plane between trajectory data points and the height h_k^a above and h_k^b below the trajectory, see Fig. 4. The area ratio is calculated as the ratio of the two areas

$$\text{Ratio} = \frac{a_a}{a_b} = \frac{\sum_{k=1}^{N} \Delta S_k h_k^a}{\sum_{k=1}^{N} \Delta S_k h_k^b}, \quad \Delta S_k = S_k - S_{k-1} \tag{1}$$

Polynomial Fit: The normalized data are averaged per trajectory groups. A polynomial model of the travel distance in the xy-plane S versus the height h is estimated. The degree of the polynomial is chosen based on the model that fits the trajectory group best.

The results of vertical component data analysis of our data are presented in Sec. 5.

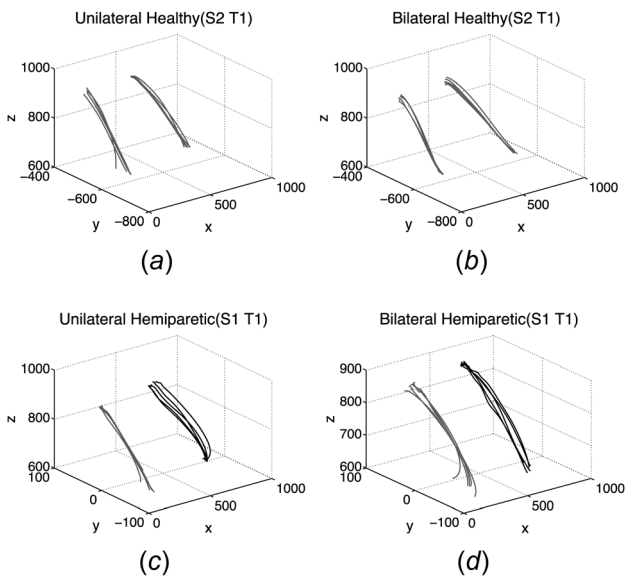

Fig. 3 Sample of the collected trajectory data relative to the motion-capturing system coordinate frame. The relative position and orientation of the target workspace with respect to the chair on which the subjects sat were kept unchanged. (*a*) Unilateral mode trajectory data of subject 2 from the control group. Both right and left trajectories are shown. (*b*) Bilateral mode trajectory data of subject 2 from the control group. (*c*) Unilateral mode trajectory data of subject 1 from the hemiparetic group. Both healthy (light gray) and unhealthy (dark gray) trajectories are shown. (*d*) Bilateral mode trajectory data of subject 1 from the hemiparetic group.

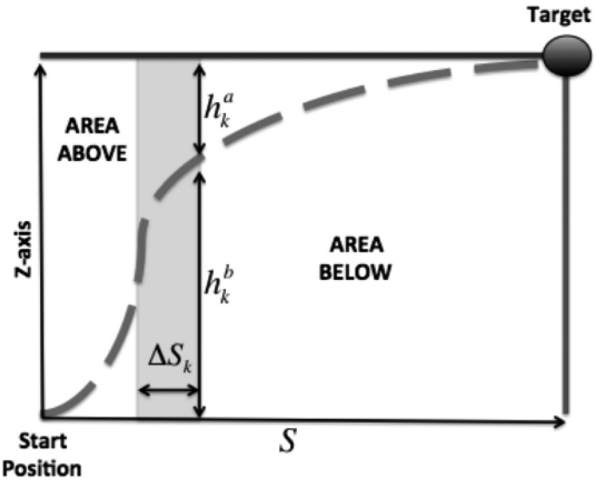

Fig. 4 Area ratio calculated as the ratio of the areas above and below the trajectory: *S* axis represents the traveled distance in the *xy*-plane, and ΔS_k are increments of the traveled distance between trajectory data points

4 MDS Analysis

In order to compare the trajectories based on their 3D shapes, here we introduce a measure of trajectory differences and apply the method of MDS. The method is capable of visualizing data in a lower dimensional space and is used for exploratory data analyses.

We apply the classical MDS method, which is based on the measure of difference a_{ij} between the trajectories i and j. The measure must be: (1) zero if the trajectories i and j are identical; (2) non-negative; and (3) symmetric, which means that the difference a_{ij} is the same as the difference a_{ji}. As a result of the MDS method, every two trajectories i and j are mapped into the points T^i and T^j of the lower dimensional space with the distance that corresponds to a_{ij}. Mathematically, the trajectories are mapped into the points as the result of the following minimization:

$$J = \min_{T^i, T^j} \sum_i \sum_{i \neq j} (a_{ij} - ||T^i - T^j||)^2 \tag{2}$$

where $||\cdot||$ corresponds to the euclidean norm of the lower dimensional space. To measure the difference between the two trajectories, we use the area between them, which can be approximated based on sampled trajectory points. This area is depicted in Fig. 5 together with the trajectories i and j and sampled points.

Figure 6(*a*) depicts two pairs of subsequent sampled trajectory positions from the trajectories i and j. The area among them can be approximated as the area S'_k of the two triangles that have the common side connecting the points $(x^i_{k+1}, y^i_{k+1}, z^i_{k+1})$ and (x^j_k, y^j_k, z^j_k). This approximation is

$$S'_k = \frac{1}{2}||\mathbf{r}^i_{k,k+1} \times \mathbf{r}^i_{k,k}|| + \frac{1}{2}||\mathbf{r}^i_{k+1,k+1} \times \mathbf{r}^j_{k,k+1}|| \tag{3}$$

where $\times$ denotes the vector product, and $||\cdot||$ the euclidean norm of a vector. However, the same area can be approximated as the area S''_k of the two triangles that have the common side connecting the points (x^i_k, y^i_k, z^i_k) and $(x^j_{k+1}, y^j_{k+1}, z^j_{k+1})$, see Fig. 6(*b*), in which case

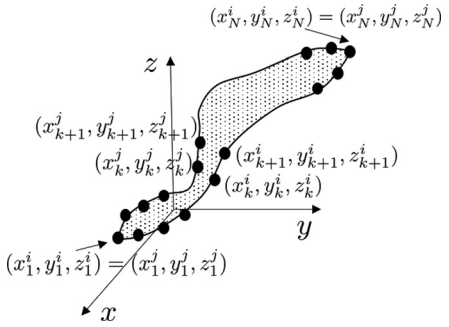

Fig. 5 Two 3D trajectories with the same number of points. The coordinates of the *k*th sample point of the *i*th and *j*th trajectories are (x_k^i, y_k^i, z_k^i) and (x_k^j, y_k^j, z_k^j), respectively. The measure of difference between the trajectories is based on the area between the trajectories (shaded).

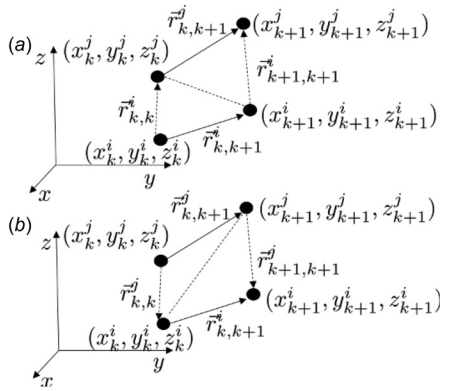

Fig. 6 Approximations of the area between two trajectories: (*a*) the area is approximated as a sum of two triangles sharing the side connecting (x_k^j, y_k^j, z_k^j) and $(x_{k+1}^i, y_{k+1}^i, z_{k+1}^i)$ and (*b*) the area is approximated as a sum of two triangles sharing the side connecting (x_k^i, y_k^i, z_k^i) and $(x_{k+1}^j, y_{k+1}^j, z_{k+1}^j)$

$$S_k'' = \frac{1}{2}||\mathbf{r}_{k,k+1}^j \times \mathbf{r}_{k,k}^j|| + \frac{1}{2}||\mathbf{r}_{k+1,k+1}^j \times \mathbf{r}_{k,k+1}^i|| \tag{4}$$

with the obvious relations $\mathbf{r}_{k,k}^i = -\mathbf{r}_{k,k}^j$ and $\mathbf{r}_{k+1,k+1}^i = -\mathbf{r}_{k+1,k+1}^j$ that are not exploited for the sake of clarity. Using the expressions for S_k' and S_k'', we define the measure of difference between the trajectories i and j as

$$a_{ij} = \sum_{k=1}^{N-1} \frac{S_k' + S_k''}{2} \tag{5}$$

which is the sum of average of the two approximations, and N is the number of sample points of each trajectory.

The measure a_{ij} defined by expression (5) is zero only if all the sampled points of the trajectories i and j are equal. It is also nonnegative and symmetric in all the cases, including the situation in which the initial and final trajectory points are not the same. However, the final trajectory points are always the same since the subjects reach the same targets. Moreover, to compensate for the variability of human subject body sizes and variability of the chair position (see Fig. 1(*a*)), we preprocess the trajectories to match the trajectory initial points. First, the final trajectory points are translated to the origin. Then, the trajectories are scaled by dividing each data point coordinate by the absolute value of the length of the trajectory along each axis

$$x_k^i = \frac{\hat{x}_k^i}{|\hat{x}_N^i - \hat{x}_1^i|}, \quad y_k^i = \frac{\hat{y}_k^i}{|\hat{y}_N^i - \hat{y}_1^i|}, \quad z_k^i = \frac{\hat{z}_k^i}{|\hat{z}_N^i - \hat{z}_1^i|} \tag{6}$$

where $\hat{x}_k^i$, $\hat{y}_k^i$, and $\hat{z}_k^i$ denote the originally recorded coordinates of the trajectory i points.

Once we compute all the mutual differences a_{ij} for a specific target, we use the MATLAB command "cmdscale" to compute an MDS map of the trajectory data for each target.

5 Results

In this section, we present data analysis results using the methods of vertical component and multidimensional scaling trajectory analyses described in Secs. 3 and 4, respectively.

5.1 Vertical Component Data Analysis. The results of the area ratio analysis of the subject groups are summarized in Fig. 7. The polynomial fit analysis results are shown in Fig. 8.

For all the targets and all the subject groups, the area ratio is below one with a 95% confidence interval. The ratios of trajectories from the hemiparetic subjects are smaller than the ratios of corresponding trajectories from the healthy subjects except in the case of targets 2 and 5 in the bilateral mode. Targets 2 and 5 have the highest median in the bilateral mode for the healthy group. In addition, there is a significant difference between the unilateral and bilateral reaching modes of the hemiparetic group for targets 2, 4, and 5 with consistently higher ratios for the bilateral reaching mode trajectories.

Assuming that the trajectory height could be modeled as the second-order polynomial, this would be an indication that the trajectory tends to have more of an upward motion at its onset. The results of the polynomial fits of the height versus distance are shown in Fig. 8. The trajectories from the healthy subjects can be modeled with the second- to the fifth-order polynomials. In both unilateral and bilateral reaching modes, the trajectories to target 2 show the lowest polynomial order, while the highest polynomial order is for trajectories in bilateral reaching mode to target 4. The trajectories from the hemiparetic subjects are more complex with polynomial orders ranging from the fourth to the eighth. The trajectories to target 2 in the bilateral mode and to target 5 in the unilateral mode are with the fourth-polynomial order. The highest eighth polynomial order is for the trajectories to target 4 of the hemiparetic subjects. These findings show that in general the trajectories cannot be modeled as the second-order polynomials. The

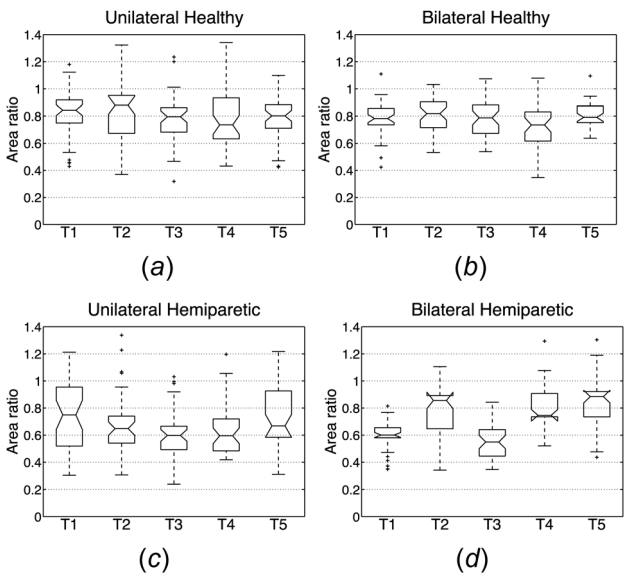

Fig. 7 Boxplots of the area ratio per target for two reaching modes and two groups of subjects. A ratio less than one means that there is an upward motion at the start of the trajectory followed by a forward motion toward the target.

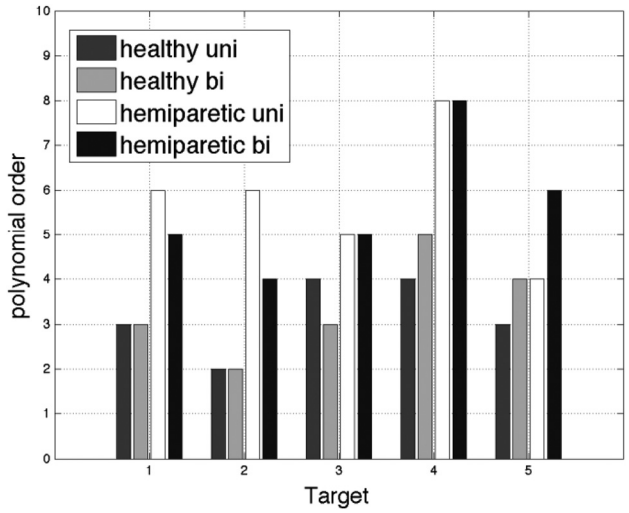

Fig. 8 The polynomial order per target for the trajectories from two reaching modes and two groups of subjects

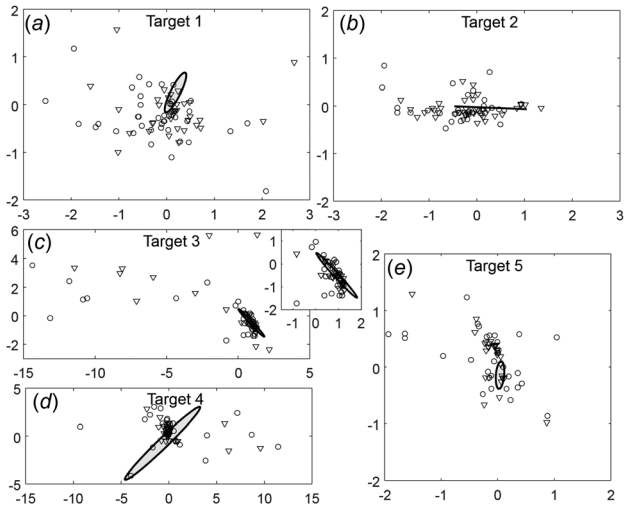

Fig. 9 The MDS maps for all the trajectories for targets 1–5 are depicted in (*a*)–(*e*), respectively: the ellipse with the shaded area describes the 95% area for the cluster of the trajectories of healthy subjects, and the points corresponding to the trajectories of hemiparetic subjects in unilateral (▽) and bilateral (○) reaching modes

trajectories to targets 2 and 5 of the hemiparetic subjects have the largest differences (which are two) in the polynomial order between the trajectories from the unilateral and bilateral reaching modes.

The trajectories of healthy subjects tend to follow a straight line toward a target in both unilateral and bilateral reaching modes. The trajectories to target 4 are excluded from this since they are somewhat similar in shape to the trajectories of hemiparetic subjects to the same target. In general, the hemiparetic trajectories are more curved, which supports the findings from the analysis of the area ratio.

5.2 MDS Analysis. The results show that most of the maps can be represented in one dimension. For a better visualization, we choose to display the maps in two dimensions.

The MDS maps of the trajectories for the five targets are shown in Fig. 9. For each target, the points corresponding to the trajectories of healthy subjects form a distinctive cluster of points in one area of the map. Instead of plotting all the points of the cluster, we depict the cluster using ellipses representing the 95% area for the points in the cluster. For each target, the ellipses are elongated and, in the case of target 2, the cluster of healthy subject trajectories is practically a line.

The points corresponding to the arm trajectories of hemiparetic subjects are spread over the map, which indicates their variability across all the subjects. The distance between a point from these subjects and the center of the healthy subject trajectory cluster can be used as a measure of how much the trajectory is "unhealthy" and to follow the progress of rehabilitation. Because of the natural variability of healthy subject trajectories, their cluster is elongated in one direction. When computing the distance, this direction needs to be taken into account with a smaller weight.

Let us consider a given target and denote all the healthy subject trajectory points with two-dimensional vectors T_h^i, $i = 1, 2, ...N_h$, where N_h is the number of healthy subject trajectories. Then, the center, i.e., the mean μ_h value and 2×2 covariance matrix Σ_h of the cluster, can be estimated as

$$\hat{\mu}_h = \frac{1}{N_h}\sum_{i=1}^{N_h} T_h^i \text{ and } \hat{\Sigma}_h = \frac{1}{N_h - 1}\sum_{i=1}^{N_h}\left(T_h^i - \hat{\mu}\right)\left(T_h^i - \hat{\mu}\right)^{\mathrm{T}} \quad (7)$$

where $\hat{}$ denotes the estimated value, i.e., $\hat{\mu}_h \approx \mu_h$, $\hat{\Sigma}_h \approx \Sigma_h$, and $^{\mathrm{T}}$ denotes the transpose of the vector. Based on the singular value decomposition (SVD), we know that the covariance matrix estimation can be represented as

$$\hat{\Sigma}_h = \Phi\Lambda\Phi^{\mathrm{T}} = \Phi\underbrace{\begin{bmatrix}\lambda_1 & 0\\ 0 & \lambda_2\end{bmatrix}}_{\Lambda}\Phi^{\mathrm{T}}, \quad \Phi^{\mathrm{T}}\Phi = I \quad (8)$$

where I is the unity 2×2 matrix, Φ is the matrix composed of unit intensity vectors aligned with the minor and major axes of the ellipse, while $\sqrt{\lambda_1}$ and $\sqrt{\lambda_2}$ are their lengths. Therefore, to measure the distance $d(p)$ between a point p of the MDS map and the center of the healthy subject cluster, we formulate the distance as

$$d(p) = ||(\sqrt{\Lambda})^{-1}\Phi^{\mathrm{T}}(p - \hat{\mu}_h)||, \quad \sqrt{\Lambda} = \begin{bmatrix}\sqrt{\lambda_1} & 0\\ 0 & \sqrt{\lambda_2}\end{bmatrix} \quad (9)$$

which can be written as

$$d(p) = \left((p - \hat{\mu}_h)^{\mathrm{T}}\underbrace{\Phi\overbrace{(\sqrt{\Lambda})^{-1}(\sqrt{\Lambda})^{-1}}^{\Lambda^{-1}}\Phi^{\mathrm{T}}}_{\Sigma_h^{-1}}(p - \hat{\mu}_h)\right)^{1/2} \quad (10)$$

and because of $\Phi^{\mathrm{T}}\Phi = I$ and $\hat{\Sigma}_h^{-1} = (\Phi\Lambda\Phi^{\mathrm{T}})^{-1} = \Phi^{\mathrm{T}}\Lambda^{-1}\Phi$, we obtain

$$d(p) = \sqrt{(p - \hat{\mu}_h)^{\mathrm{T}}\hat{\Sigma}_h^{-1}(p - \hat{\mu}_h)} \quad (11)$$

If we introduce $\hat{\mu}_{\mathrm{uni}}$ and $\hat{\mu}_{\mathrm{bi}}$ as the centers of the clusters of hemiparetic subject trajectories in unliateral and bilateral reaching modes, then their center distances to the center of healthy subject trajectory cluster are $d(\hat{\mu}_{\mathrm{uni}})$ and $d(\hat{\mu}_{\mathrm{bi}})$, respectively.

These distances are presented in Fig. 10(*a*) for each target. From it, we can find that the largest one is for target 3 and that in all the other cases, the distances are comparable, which is in agreement with Fig. 9 showing that the points corresponding to hemiparetic subject trajectories in unilateral and bilateral modes overlap with the healthy ones except in the case of target 3, where the unilateral mode trajectories are dispersed all over the map, see Fig. 9(*c*).

To get a quantitative insight into the variability of trajectories, we compute the standard deviations of trajectory points over a certain distance from the center of the healthy subject trajectory

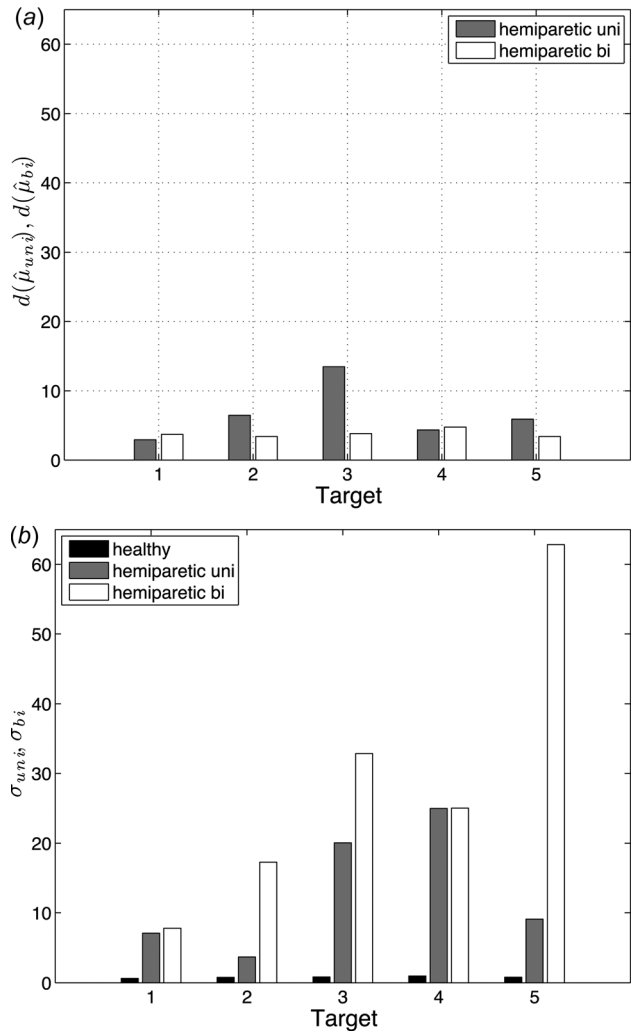

Fig. 10 The distances of the centers of points corresponding to the unilateral and bilateral hemiparetic trajectories to the center of the healthy subject cluster (*a*) and the standard deviation (*b*) of the distance to the center of the healthy trajectory cluster. The bar graphs show the distances and standard deviation per type of the trajectory and target.

cluster. We first compute $d(T^i)$ for any point representing a trajectory from the group of unilateral trajectories and then compute the standard deviation σ_{uni} of the distance

$$\sigma_{\text{uni}} = \sqrt{\frac{1}{N_{\text{uni}}-1}\sum_{i=1}^{N_{\text{uni}}}(d(T^i)-\bar{d}_{\text{uni}})^2},\ \ \bar{d}_{\text{uni}} = \frac{1}{N_{\text{uni}}}\sum_{i=1}^{N_{\text{uni}}} d(T^i) \tag{12}$$

where $\bar{d}_{\text{uni}}$ is the mean value of the distance. Similarly, we compute the standard deviation σ_{bi} of the distance

$$\sigma_{\text{bi}} = \sqrt{\frac{1}{N_{\text{bi}}-1}\sum_{i=1}^{N_{\text{bi}}}(d(T^i)-\bar{d}_{\text{uni}})^2},\ \ \bar{d}_{\text{bi}} = \frac{1}{N_{\text{bi}}}\sum_{i=1}^{N_{\text{bi}}} d(T^i) \tag{13}$$

for bilateral trajectories. The standard deviations for each target are presented in Fig. 10(*b*). We note that the dispersion of the points in the healthy subject cluster is the smallest, which is also supported by Fig. 9 across all the targets. We can also confirm that the dispersion of target 3 unilateral trajectories is comparable to their distance in Fig. 10(*a*), which is also in agreement with the map in Fig. 9(*c*).

From Fig. 10(*b*), it follows that the variability of trajectories is comparable among unilateral and bilateral trajectory types for targets 1 and 4. A significant difference in the variability in these types of trajectories is observed in target 5 with the pattern of more variable bilateral trajectories than unilateral trajectories. The same pattern can be also clearly seen for targets 2 and 3. However, targets 3 and 4 have consistently high variabilities in both modes, which means that for these targets the hemiparetic subjects consistently express a high level of unhealthy synergies in their motion.

Overall, Figs. 9 and 10 show that the major difference between the trajectories of hemiparetic and healthy subjects is in a strong consistency of the second ones for each target, which is illustrated well by their MDS map clusters of points. In other words, all the healthy subject trajectories are similar to each other. Such a level of similarity does not exit among the hemiparetic subject trajectories since they are typically dispersed over the MDS maps.

However, once we focus on a specific subject from the hemiparetic group, we can find its MDS trajectory points less dispersed over the map, which indicates consistency in motion. For example, subject 2's MDS maps per target are shown in Fig. 11. The maps for targets 1–5 show an obvious dissimilarity of the subject's trajectories in unilateral and bilateral reaching mode since the corresponding MDS points are easily separable. In the case of targets 3 and 4, the MDS trajectory points for both modes, with a few exceptions, overlap with the clusters of the healthy subject trajectories. If this happened for all the targets, we would conclude that subject 2 is fully recovered. However, the MDS maps for targets 1, 2, and 5 show that the subject's reaching trajectories for these targets are different from the healthy. Interestingly enough, subject 2 belongs to the group of hemiparetic subjects and, for targets 3 and 4, the group shows consistently the largest dispersions of the MDS map points in both reaching modes. This indicates the importance of individual therapy plans since the high level of unhealthy synergies of the hemiparetic group for targets 3 and 4 is not characteristic of subject 2's trajectories.

From this, for example, we can conclude that subject 2 should have a therapy that would emphasize motions necessary to reach targets 1, 2, and 5. In that case, we would also give a slight preference to a therapy that engages two arms simultaneously because of considerably larger distances of the MDS map points for target 2 in the bilateral reaching mode.

Naturally, the impact of our analysis to therapy planning is speculative in nature and should be further investigated. However,

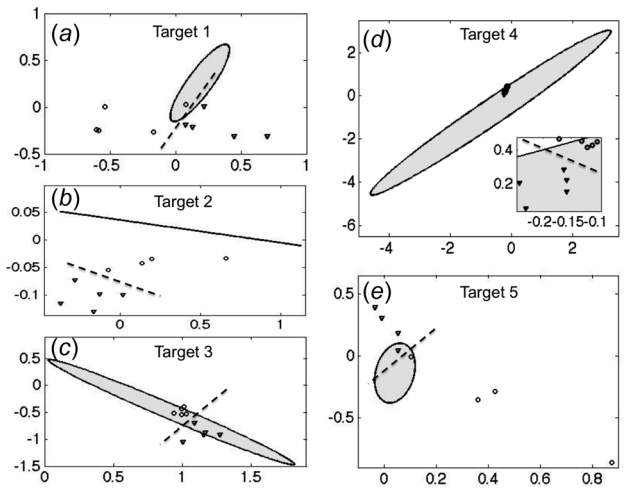

Fig. 11 Subject 2 map for all the targets are shown in (*a*)–(*e*). (▽) represents the bilateral trajectories, and (○) represents the unilateral reaching trajectories of subject 2. The dashed lines illustrate the separation between the unilateral and bilateral trajectories. The ellipses with the shaded areas describe the 95% area for the cluster of healthy trajectories.

we clearly show that for a specific subject our analysis can pinpoint specific targets creating problems in reaching motions.

6 Discussion

Although the polynomial fit method indicates that *z*-axis profile trajectories are more complex than the second-order polynomials, both area ratio and polynomial fit analyses are in agreement that trajectories tend to move upward on the onset and then forward. Based on the area ratio, the trajectories to targets 2 and 5 have the biggest departure from that pattern especially in bilateral reaching mode. While the position of targets plays a critical role, the latter can be explained only by a higher demand on subject's attention [27], which impacts visual and proprioceptive feedbacks contributing to reaching motions. The *z*-axis profile analyses also show that the trajectories of hemiparetic subjects have a higher-order polynomial model than the trajectories of healthy subjects. The highest-order polynomial model is required for hemiparetic bilateral reaching mode trajectories. This can be explained by both muscular weakness and unhealthy synergies [16,28–31] that result into more complex reaching trajectory patterns. While these may be useful results, the overall attempt to analyze the data along the *z*-axis does not show the potential to reveal characteristics of individual subject trajectories.

With the aim to use complete 3D data about the trajectories, we introduced the area between two trajectories as a measure of their dissimilarity and explored the data using the MDS method. The method was applied to hemiparetic and healthy subject trajectories in both reaching modes and resulted in the MDS maps with up to two dimensions for each target. The MDS maps showed that, contrary to the healthy subject trajectories, the hemiparetic subject trajectories did not group into distinctive clusters, which means that they are all different from each other.

The differences between unilateral and bilateral reaching mode trajectories of the hemiparetic subject group are evident from Fig. 10(*b*). It shows that unilateral mode hemiparetic subject trajectories are consistently closer to the healthy than the trajectories from the bilateral mode. Also, the farther ipsilaterally the target is, the higher the variability of unilateral mode trajectories of the hemiparetic subjects is. The highest variability of trajectories is in bilateral reaching mode of the hemiparetic subjects for target 5. However, targets 3 and 4 have consistently high variabilities in both modes. This characteristic does not show in the analysis of subject 2 that belongs to the hemiparetic group and based on this we can conclude that the therapy for subject 2 cannot be equal to the other subjects of the same group. By this, we underline the importance of individual subject analyses and therapy plans.

MDS analyses not only reveal the dissimilarity structure of the trajectory groups but also provide an insight into the variability of subject trajectories per target by measuring the dispersion of the MDS points per trial of a subject. The significance of variability is in the evaluation of the strategy that an individual is using in the process of recovery. The strategies can be compensatory in nature or reflect true recovery. Compensatory strategies are employed to accomplish daily activities, however, this hinders true recovery in that it disregards the training of natural joint configurations [32–34].

When multiple trajectories of one patient to a specific target are represented in the MDS map, they form a set which can be compared to the cluster of points corresponding to the healthy subjects, and there are three outcomes that can be identified: (1) the patient's set has a low dispersion and overlaps with the cluster of healthy subjects, which indicates the fully recovered patient; (2) the patient's set has a low dispersion and it does not overlap with the cluster of healthy subjects, which indicates that the patient is functionally recovered, i.e., has consistent trajectories, but uses a compensatory motion strategy resulting in trajectories that are different from those of the healthy subjects; and (3) the patient's set has a high dispersion, with or without the overlap with the cluster of healthy subjects, which indicates the inconsistency of motion associated with an early phase of or nonresponsiveness to the therapy. The size of overlap between the patient's set and the cluster of healthy subjects measures only a degree of dissimilarity of the patient's trajectories to the healthy subject trajectories.

In spite of the data reduction resulting from the MDS map, a therapist may have access to the original trajectory while comparing it with trajectories of healthy subjects. The *z*-axis component of the trajectory may provide an insight regarding muscle strength compensating gravitational loads, while the *xy*-components of the trajectory provide information regarding the muscular coordination during the reaching task. Assessing in this context may affect the treatment regime that is unique to each patient under evaluation. As the patient progresses through the rehabilitation treatment, it is anticipated that the dispersion of the MDS points will provide a quantitative measure of the progress, while their distance to the cluster of healthy trajectories will indicate the direction of the progress toward a full or functional recovery.

7 Conclusion

Our aim to quantitatively analyze hand trajectories has led us to the novel method of characterizing the trajectories by using the MDS. With the MDS, we were able to generate the map that visualizes dissimilarities between the trajectories in a two-dimensional space. In the map, each trajectory is represented by a point and the healthy subject trajectories are mapped into a distinctive cluster of points. The analysis of the MDS points provided us the valuable insight into the differences among the trajectory groups and the variability of group trajectories. In order to identify the level of accuracy of this quantitative, data-driven objective tracking in the context of standard expert-based, subjective assessment methods such as FMA, or WMFT, it is necessary to perform a larger study, which can be a part of our future work.

Quantifying the differences and variabilities of trajectory groups is significant because it can guide therapists in establishing different therapeutic plans. For example, a high variability of trajectories in a reaching task to a target can be used to emphasize the part of therapy that will decrease their variability. After a period in the therapy, the therapist can use the MDS map to detect if the subject uses compensatory strategies or shows the progress toward true recovery. With this, the effectiveness of the therapy can be evaluated and the therapist can potentially use it to steer the direction of the rehabilitation plan.

References

[1] Dariush Mozaffarian, D., Benjamin, E. J., Go, A. S., Arnett, D. K., Blaha, M. J., Cushman, M., de Ferranti, S., Després, J.-P., Fullerton, H. J., Howard, V. J., Huffman, M. D., Judd, S. E., Kissela, B. M., Lackland, D. T., Lichtman, J. H., Lisabeth, L. D., Liu, S., Mackey, R. H., Matchar, D. B., McGuire, D. K., Mohler III, E. R., Moy, C. S., Muntner, P., Mussolino, M. E., Nasir, K., Neumar, R. W., Nichol, G., Palaniappan, L., Pandey, D. K., Reeves, M. J., Rodriguez, C. J., Sorlie, P. D., Stein, J., Towfighi, A., Turan, T. N., Virani, S. S., Willey, J. Z., Woo, D., Yeh, R. W., and Turner, M. B., 2015, "Heart Disease and Stroke Statistics 2015 Update: A Report From the American Heart Association," Circulation, **29**(322), pp. e29–e322.

[2] Stinear, C., Barber, P., Smale, P. R., Coxon, J. P., Fleming, M. K., and Byblow, W. D., 2007, "Functional Potential in Chronic Stroke Patients Depends on Corticospinal Tract Integrity," Brain, **130**(Pt. 1), pp. 170–180.

[3] Hsieh, C. L., Hsueh, I. P., Chiang, F. M., and Lin, P. H., 1998, "Inter-Rater Reliability and Validity of the Action Research Arm Test in Stroke Patients," Age Ageing, **27**(2), pp. 107–113.

[4] Platz, T., Pinkowski, C., van Wijck, F., Kim, I. H., Bella, P. D., and Johnson, G., 2015, "Reliability and Validity of Arm Function Assessment With Standardized Guidelines for the Fugl-Meyer Test, Action Research Arm Test and Box and Block Test: A Multicentre Study," Clin. Rehabil., **19**(4), pp. 401–411.

[5] Kopp, B., Kunkel, A., Flor, H., Platz, T., Rose, U., Mauritz, K. H., Gresser, K., McCulloch, K. L., and Taub, E., 1997, "The Arm Motor Ability Test: Reliability, Validity, and Sensitivity to Change of an Instrument for Assessing Disabilities in Activities of Daily Living," Arch. Phys. Med. Rehabil., **78**(6), pp. 615–620.

[6] Bohannon, R. W., and Smith, M. B., 1987, "Interrater Reliability of a Modified Ashworth Scale of Muscle Spasticity," Phys. Ther., **67**(2), pp. 206–207.

[7] Cushman, L. A., and Scherer, M. J., 1996, "Measuring the Relationship of Assistive Technology Use, Functional Status Over Time, and Consumer Therapist Perceptions of ATS," Assistive Technol., **8**(2), pp. 103–109.

[8] Baptiste, S., Carswell, A., McColl, M. A., Polatajko, H., and Pollock, N., 2014, "Canadian Occupational Performance Measure (COPM)," Canadian Association of Occupational Therapists (CAOT), Ottawa, ON, Canada.
[9] Van der Lee, J. H., Beckerman, H., Lankhorst, G. J., and Bouter, L. M., 2001, "The Responsiveness of the Action Research Arm Test and the Fugl-Meyer Assessment Scale in Chronic Stroke Patients," J. Rehabil. Med., **33**(3), pp. 110–113.
[10] Van der Lee, J. H., Beckerman, H., Knol, D. L., de Vet, H. C., and Bouter, L. M., 2004, "Clinimetric Properties of the Motor Activity Log for the Assessment of Arm Use in Hemiparetic Patients," Stroke, **35**(6), pp. 1410–1414.
[11] Poole, J. L., and Whitney, S. L., 1988, "Motor Assessment Scale for Stroke Patients: Concurrent Validity and Interrater Reliability," Arch. Phys. Med. Rehabil., **69**(3Pt. 1), pp. 195–197.
[12] Mathiowetz, V., Weber, K., Kashman, N., and Volland, G., 1985, "Adult Norms for the Nine Hole Peg Test of Finger Dexterity, OTJR: Occupation," Participation Health, **5**(1), pp. 24–38.
[13] Morris, D. M., Uswatte, G., Crago, J. E., Cook, E. W., and Taub, E., 2001, "The Reliability of the Wolf Motor Function Test for Assessing Upper Extremity Function After Stroke," Arch. Phys. Med. Rehabil., **82**(6), pp. 750–755.
[14] Gladstone, D., Daniels, C., and Black, S., 2002, "The Fugl-Meyer Assessment of Motor Recovery After Stroke: A Critical Review of Its Measurement Properties," Am. Soc. Neurorehabil., **16**(3), pp. 232–240.
[15] Duncan, P., Propst, M., and Nelson, S., 1983, "Reliability of the Fugl-Meyer Assessment of Sensorimotor Recovery Following Cerebrovascular Accident," Phys. Ther., **63**(10), pp. 1606–1610.
[16] Simkins, M., Al-Refai, A., and Rosen, J., 2014, "Upper Limb Joint Space Modelling of Stroke Induced Synergies Using Isolated and Voluntary Arm Perturbations," IEEE Trans. Neural Syst. Rehabil. Eng., **22**(3), pp. 491–500.
[17] Krakauer, J., 2006, "Motor Learning: Its Relevance to Stroke Recovery and Neurorehabilitation," Curr. Opin. Neurol., **19**(1), pp. 84–90.
[18] Levin, M., Kleim, J., and Wolf, S., 2009, "What Do Motor 'Recovery' and 'Compensation' Mean in Patients Following Stroke?" Neurorehabil. Neural Repair, **23**(4), pp. 313–319.
[19] Borg, I., Groenen, P., and Mair, P., 2013, *Applied Multidimensional Scaling*, Springer, New York.
[20] Borg, I., and Groenen, P., 2005, *Modern Multidimensional Scaling (Theory and Applications)*, Springer, New York.
[21] Kuiken, C., DeJong, J., Baan, E., Keulen, W., Tersmette, M., and Goudsmit, J., 1992, "Evolution of the v3 Envelope Domain in Proviral Sequences and Isolates of Human Immunodeficiency Virus Type 1 During Transition of the Viral Biological Phenotype," J. Virol., **66**(7), pp. 4622–4627.
[22] Bedford, T., Suchard, M., Lemey, P., Dudas, G., Gregory, V., Hay, A. J., McCauley, J. W., Russell, C. A., Smith, D. J., and Rambaut, A., 2014, "Integrating Influenza Antigenic Dynamics With Molecular Evolution," Elife, **3**, p. e01914.
[23] He, J., and Deem, M., 2010, "Low-Dimensional Clustering Detects Incipient Dominant Influenza Strain Clusters," Protein Eng. Des. Sel., **23**(12), pp. 935–946.
[24] Smith, D., Lapeded, A., de Jong, J., Bestebroer, T. M., Rimmelzwaan, G. F., Osterhaus, A. D., and Fouchier, R. A., 2004, "Mapping the Antigenic and Genetic Evolution of Influenza Virus," Sci. Mag., **305**, pp. 371–376.
[25] Vicon Industries, 2015, "Motion Capture on the WWW," http://www.vicon.com/
[26] Vicon, 2015, "Vicon BodyBuilder Manual," Vicon Industries, Oxford, UK.
[27] Harley, L., 2011, "Stages in Learning Motor Synergies: A View Based on the Equilibrium-Point Hypothesis," Ph.D. thesis, School of Applied Physiology, Georgia Institute of Technology, Atlanta, GA.
[28] Ada, L., Canning, C., and Low, S., 2003, "Stroke Patients Have Selective Muscle Weakness in Shortened Range," Brain, **126**(Pt. 3), pp. 724–731.
[29] Bohannon, R., 2007, "Muscle Strength and Muscle Training After Stroke," J. Rehabil. Med., **39**(1), pp. 14–20.
[30] Dewald, J., Pope, P., Given, J., Buchanan, T. S., and Rymer, W. Z., 1995, "Abnormal Muscle Co-Activation Patterns During Isometric Torque Generation at the Elbow and Shoulder in Hemiparetic Subjects," Brain, **118**(Pt. 2), pp. 495–510.
[31] Dewald, J., and Beer, R., 2001, "Abnormal Joint Torque Patterns in the Paretic Upper Limb of Subjects With Hemiparesis," Muscle Nerve, **24**(2), pp. 273–283.
[32] Ada, L., Canning, C., Carr, J. H., Kilbreath, S. L., and Shepherd, R. B., 1994, "Task Specific Training of Reaching and Manipulation," Adv. Psychol., **105**, pp. 239–265.
[33] Cirstea, C., Ptito, A., Forget, R., and Levin, M. F., 2000, "Arm Motor Improvement in Stroke Patients May Depend on Type of Training," Soc. Neurosci. Abstr., **26**(1–2).
[34] Roby-Brami, A., Feydy, A., Combeaud, M., Biryukova, E. V., Bussel, B., and Levin, M. F., 2003, "Motor Compensation Recovery for Reaching in Stroke Patients," Acta Neurol. Scand., **107**(5), pp. 369–381.